SUPPLEMENTARY MATERIALS

- **Origin of the reduced velocity in the mantle lithosphere**

Here we discuss a few mechanisms under which shear-wave velocity can be reduced within the lithospheric mantle including thermal effects, extensional deformation, and intrusion of magmatic melts. Although each of these processes is considered individually, they are not mutually exclusive. Temperature has a negative effect on elastic modulus and thus a positive thermal anomaly in the asthenosphere could lead to reduction in shear-wave velocity in the overlying mantle lithosphere. Isolated negative Vs anomalies at various depths in the region of boudinage have been identified from several studies (Krauss et al., 2020; Yao and Li, 2016; Zhu et al., 2020). Some of these studies attributed the anomalies to a thermal source in the mantle, even though the exact nature of such a thermal source has not been identified. The GoM was speculated to have formed as a back-arc basin above mantle return-flow associated with the subduction zone in western Mexico (Stern et al., 2010). To examine the probability of thermally-induced Vs reduction, we used the derivative relationship between temperature and shear-wave velocity of -3.75 x 10-4 km s^{-1} $^{o}C^{-1}$ (Liu et al., 2005) to estimate the thermal anomalies at depths of 75 and 150 km (Supplementary Fig. 5). The result shows that the Vs reduction observed within the mantle lithosphere under the GoM margin would require a temperature variation of >150^{o}C at 75 km depth relative to the extended lithosphere onshore North America, while at 150 km depth the thermal anomaly required is only ~25^{o}C. A thermal anomaly on the scale of 150^{o}C seems unrealistic at this shallow depth in a passive margin where seafloor spreading ceased more than 135 million years ago. . It is also difficult to envision how a thermal plume would give rise to corrugation in the mantle lithosphere. The observed reduction in Vs in the boudin necking regions is therefore unlikely to be associated with an anomalous mantle heat source.

Imaging of boudin structures in the lithospheric mantle strongly supports extensional deformation as the velocity reducing process. Stretching of a rheologically layered body results in instability of the strong, competent layer that deforms into the discrete lozenges making up the boudins. While this phenomenon is mostly seen on smaller scales, lithospheric boudinage has been suggested in the Basin and Range Province (Froidevaux et al., 1986; Fletcher and Hallet, 1983) and the western Mediterranean basin (Gueguen et al., 1997). Furthermore, mantle rock under extensional stress becomes rheologically weaker due to the transition from dislocation to diffusion creep as the dominant deformation mechanism (Karato and Wu, 1993; Yamasaki, 2004) and experiences grain size reduction resulting in reduced shear modulus (Faul and Jackson, 2005; Jackson et al, 2001). Hence, both geologic boudinage and velocity reduction can be enhanced in the extensional continental rifting setting or within a subducting slab. Numerical models have attributed both subducting plate segmentation and reduced seismic velocity to grain-size reduction (Gerya et al., 2021).

We attribute the largest reduction in Vs observed in the boudin necks to development of localized shear zones during rifting. While geologic boudinage reported within the sedimentary layers is commonly formed by viscosity stratification, the observed lithospheric boudinage most likely formed by shear zones localized by mantle heterogeneity. This conclusion is drawn from using the apparent length and thickness of the boudinage and estimating the viscosity ratio (Smith, 1977) between the mantle lithosphere and asthenosphere. This estimate produces a ratio of ~1.3, significantly less than the expected two-order of magnitude viscosity contrast across the lithosphere-asthenosphere boundary. We, therefore, infer that localized shear zones could lead to

further grain-size reduction by dynamic recrystallization during extension that further weakened the mantle lithosphere. Hence, the necking regions of the boudins become areas with the most deformation and lowest shear-wave velocity. At 1300^{o}C a grain size reduction from 10 mm to 1mm, the maximum threshold where diffusion creep can be established (Hopper and Buck, 1993), would lead to a ~10% decrease in shear modulus (Faul and Jackson, 2005). This amounts to a Vs reduction of ~5% which is the same order of magnitude with the observed 1-3% reduced Vs in the mantle boudinage. We infer that during the Triassic-Jurassic rifting event the mantle lithosphere experienced a drop in its shear modulus and hence shear velocity by a number of related extensional processes, which ultimately led to formation of localized shear zones now defining the boudinage necks.

Finally, we consider a scenario in which Vs of the mantle lithosphere is reduced by the effect of melt intrusion. Decompression melting at the top of the asthenosphere as the lithosphere was stretched and thinned during rifting could have generated melts that infiltrated the overlying mantle lithosphere. Distributed partial melts by themselves can reduce the Vs of the mantle, but due to their low volume below normal or even thinned continental lithosphere they are normally expected to rise through the lithosphere, intrude the crust and/or erupt at the surface. In that case, the negative effect on Vs of partial melts in the lithosphere would be transient. However, if magmatic melts are trapped in the mantle lithosphere (Pérez-Gussinyé et al, 2006; Müntener et al., 2009) and react with the host rock, metasotamism will take place. This is a process of mantle refertilization during which the depleted harzburgite in the lithosphere is re-enriched to lherzolite (O'Reilly and Griffin, 2013; Foley, 2008). As a result, the mantle lithosphere becomes denser but exhibits a lower seismic velocity and a weaker rheology with decreased elastic thickness. Evidence from petrological studies has shown that mantle metasomatism occurred in both cratonic (Casagli et al., 2017; Griffin et al., 2009; Wang et al., 2015) and non-cratonic environments as well as oceanic regions (O'Reilly and Griffin., 2013; Ranalli et al., 2007). In the GoM, evidence for rejuvenation of the mantle lithosphere during Mesozoic rifting was found in mantle xenoliths collected along the coast of Louisiana (Stern et al., 2011). Radiometric dating confirms the age of these sample at ~160.1 Ma, near the end of continental rifting. Furthermore, trace element analysis indicates a history of mantle enrichment and low-degree of melting, raising the possibility of mantle metasomatism due to melt-rock interaction during the Mesozoic extension. It is likely that the observed reduction in Vs from our model results from the combined effects of extensional deformation and mantle refertilization during rifting.

Supplementary Figure 1: **a)** Location map displaying distribution of seismic stations used for ambient noise cross-correlation. Green triangles denote long-term stations. Red dots are temporary stations. The data from the following networks were obtained from IRIS: including the following seismic networks: (1) the TA (Transportable Array; IRIS, 2003); (2) the US (USNSN, Albuquerque, 1990); (3) the IU (GSN; Albuquerque, 1988); (4) the TX (BEG, The University of Texas at Austin, 2016); (5) the Z9 (Fischer et al., 2010); (6) the TO (MASE, 2007); (7) the N4 (ASL, 2013); (8) the CU (ASL, 2006); (9) the CW (CENAIS, Cuba, 1998). Calculated correlation-pairs are shown in grey dashes **b)** Checkerboard test in a half-degree grid showing sufficient resolution provided by the ray-path coverage at period 40 s. Results from other periods have similar resolution. The input velocity anomalies are ±5%.

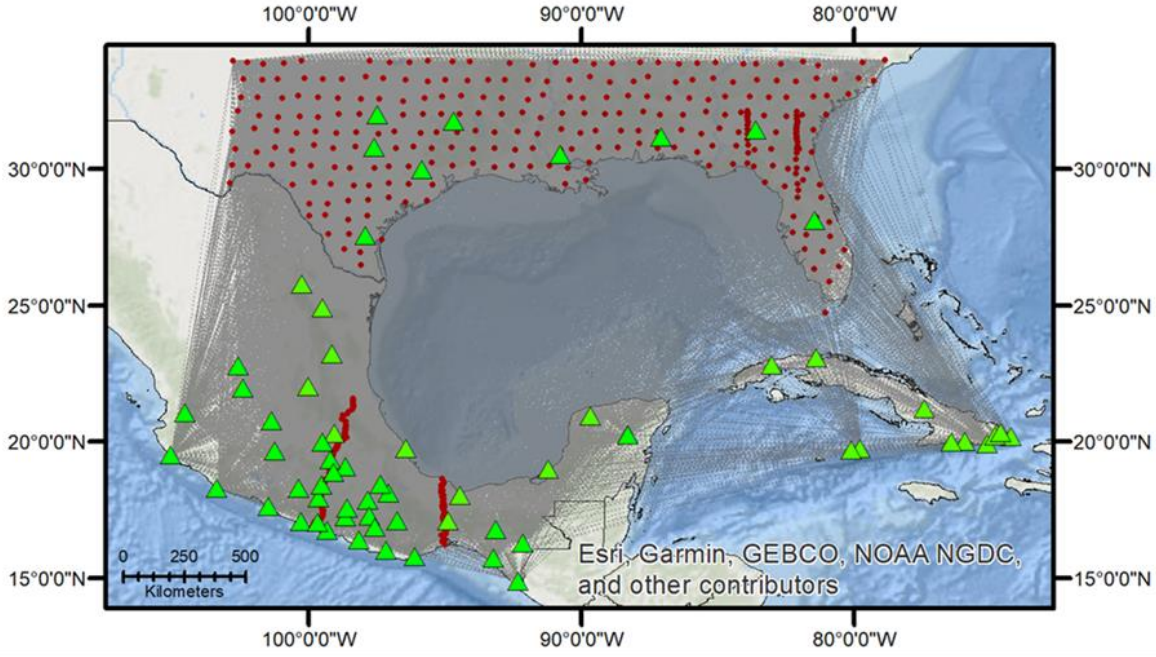

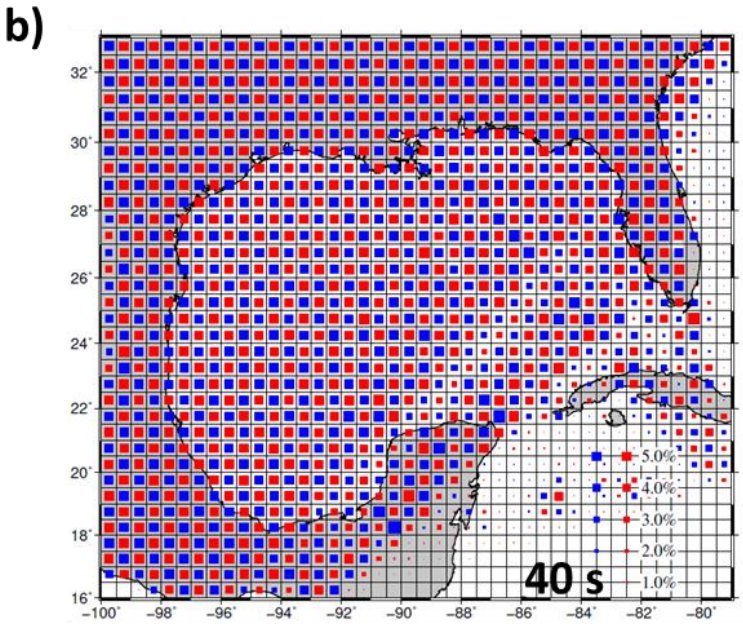

Supplementary Figure 2: Comparison of our velocity model and Moho depths (white lines) from previous seismic refraction studies **a)** Van Avendonk et al. (2015) **b)** Eddy et al. (2018) **c)** Eddy et al. (2014) **d)** Christeson et al. (2014). Our estimate of Moho depths follows the 4.2 km/s contour (white dashes). The misfit averaged along all four profiles is ~2.5 km.

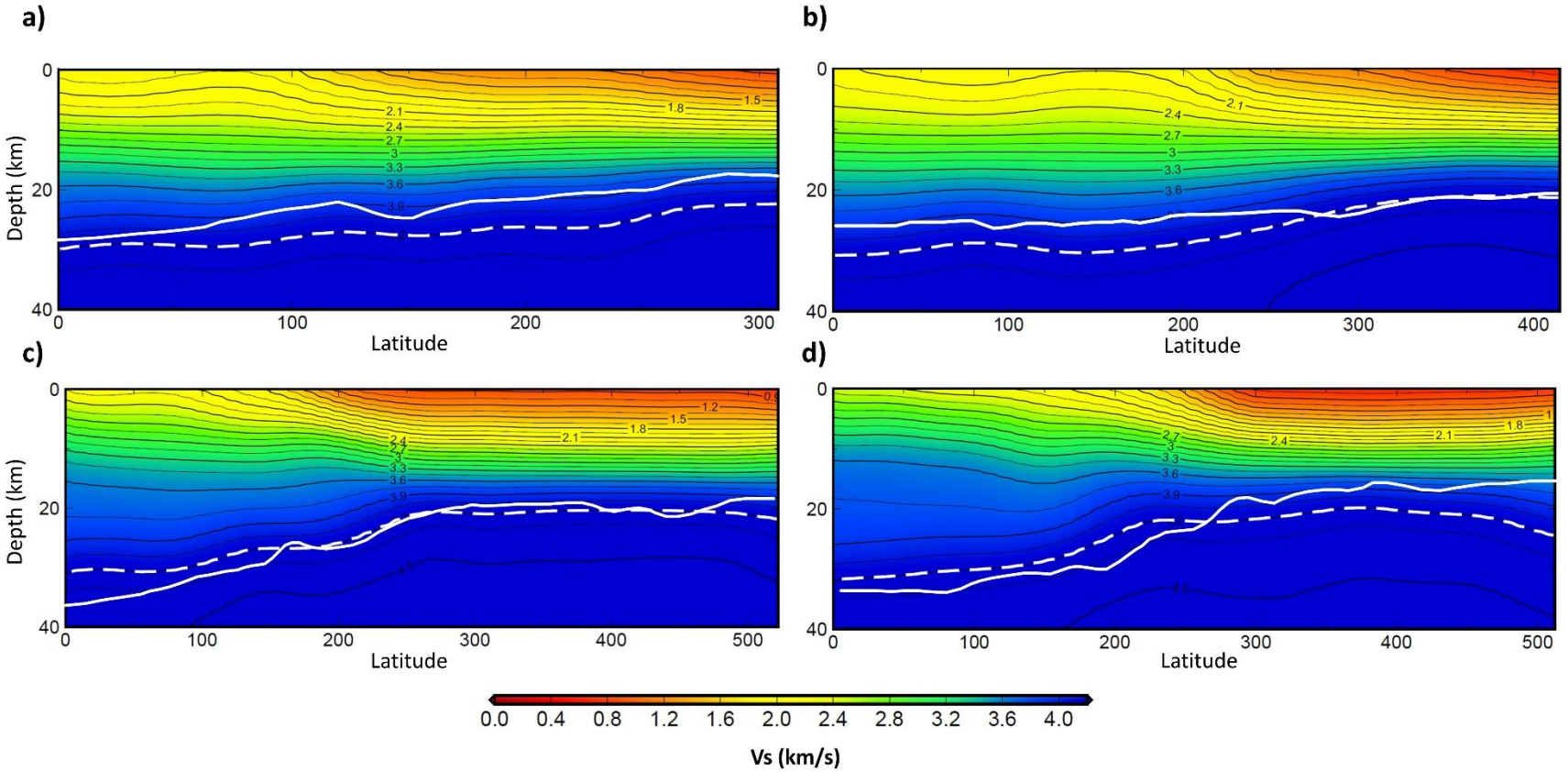

Supplementary Figure 3: Measured dispersion curves at various grid points over the pinch and swell areas of the observed lithospheric boudinage. Phase velocities over the pinch zones (red lines/markers) are consistently lower than that of the swell areas (black lines/markers). Measurement uncertainty (~1%) approximates markers' size. Phase velocities over an onshore location is shown in grey for reference. Numbers in parentheses denote latitudes and longitudes at grid nodes.

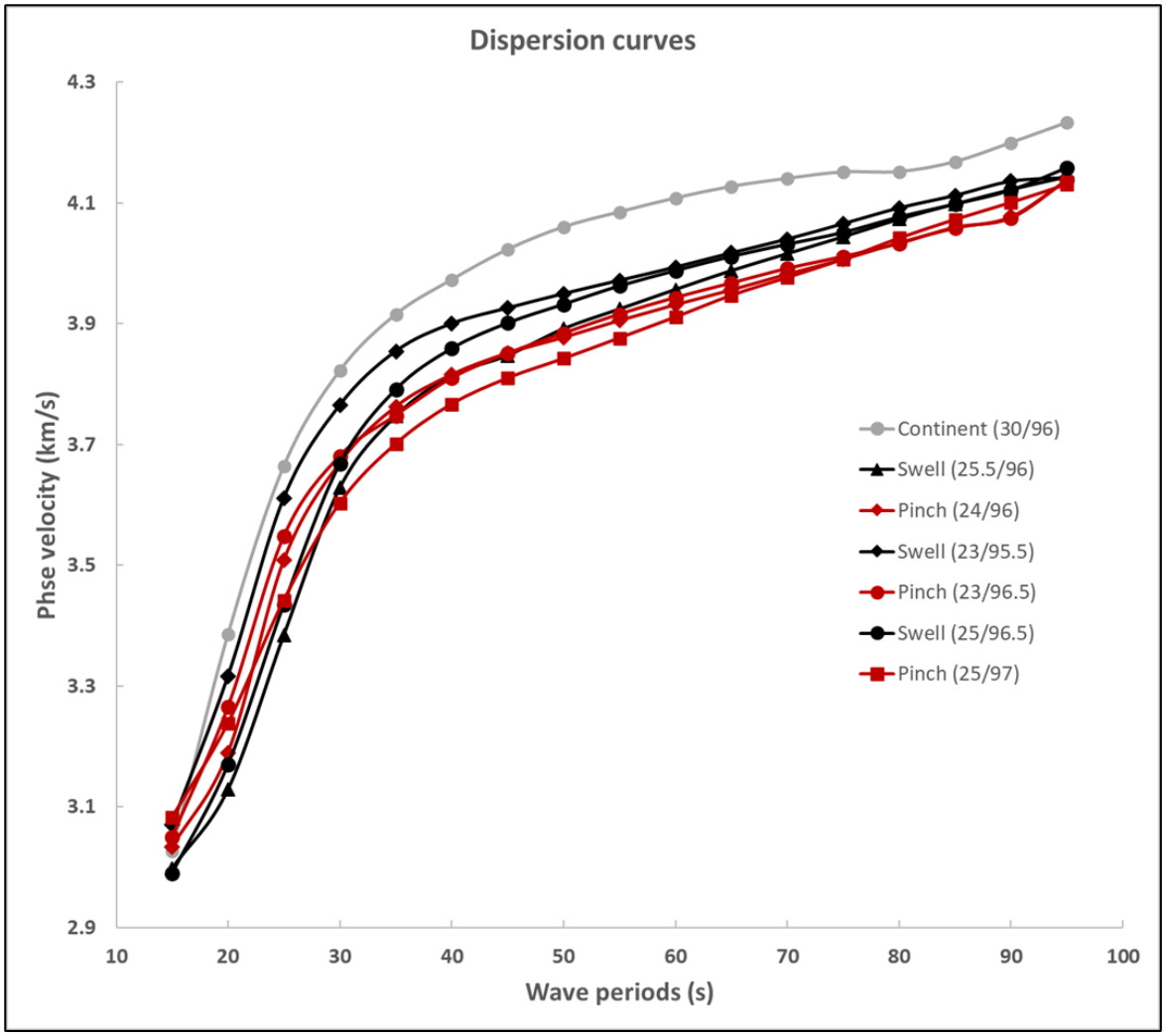

Supplementary Figure 4: We tested the phase velocity sensitivity with depth to constrain the vertical extent of the zone of reduced Vs. Dispersion data are from a grid node within the region of mantle Vs reduction and boudinage. During inversion of the Test model, mantle Vs is fixed at 4.7 km/s while crustal Vs varies between 3.0-4.0 km/s. Moho depth is constrained within a wide range of 20 km. The results show that varying crustal Vs and Moho depth cannot compensate for the misfits at wave periods above 40 s. Our preferred model, which allows mantle Vs to fluctuate between 4.3 and 4.7 km/s, produces a better fit with the observed data. This result is consistent throughout the area of reduced mantle Vs in the offshore northwestern GoM. Tables 1 and 2 summarize the misfits from these two models at eight grid nodes in the boudinage zone.

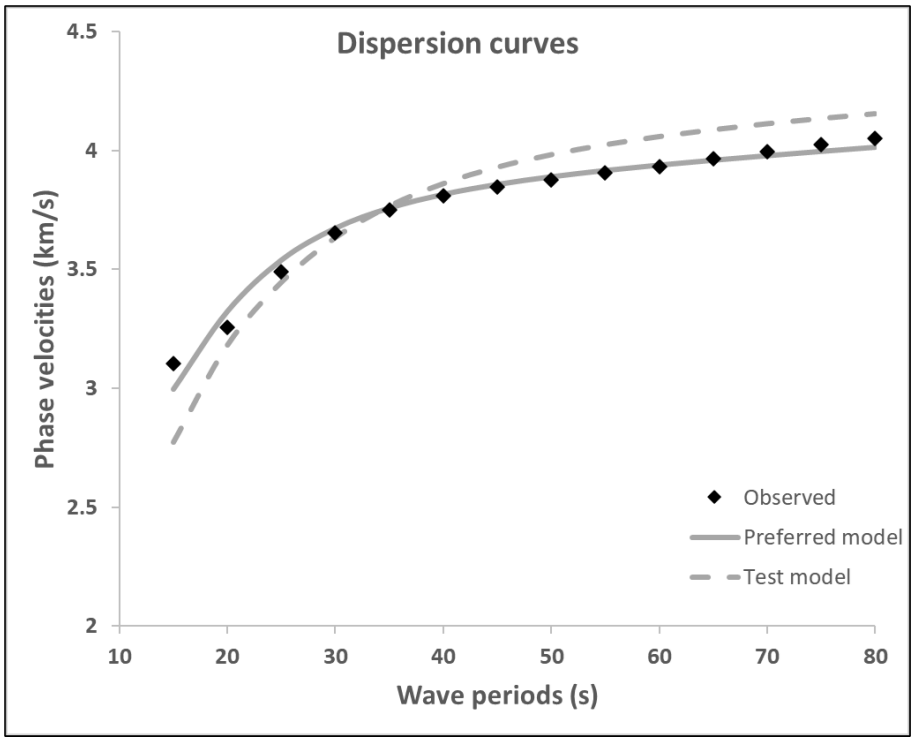

Supplementary Table 1: Misfits of phase velocities from the preferred model at eight inversion nodes in the region of reduced Vs. The overall misfit is less than 1%.

Wave Periods	Percent Misfit at Inversion Nodes (longitude/latitude)								Average Misfit (%)
	95.5/23.5	96/24	96.5/24.5	97/25	95.5/25.5	96/26	96.5/26.5	97/27	
40	-0.30	0.00	0.05	-0.49	0.79	0.13	0.41	0.22	**0.30**
45	-0.36	-0.20	0.01	-0.54	0.49	0.25	0.55	0.54	**0.37**
50	-0.27	-0.20	0.11	-0.39	0.44	0.37	0.84	0.79	**0.43**
55	-0.16	-0.15	0.29	-0.14	0.35	0.61	0.97	1.00	**0.46**
60	0.15	-0.09	0.54	0.21	0.41	0.87	1.13	1.24	**0.58**
65	0.40	0.05	0.75	0.43	0.42	1.15	1.28	1.52	**0.75**
70	0.70	0.19	1.00	0.69	0.37	1.30	1.31	1.69	**0.91**
75	0.89	0.42	1.28	1.09	0.53	1.54	1.54	1.93	**1.15**

Supplementary Table 2: Misfits of phase velocities from the Test model at eight inversion nodes in the region of reduced Vs. The overall misfit is >2.5%.

Wave Periods	Percent Misfit at Inversion Nodes (longitude/latitude)								Average Misfit (%)
	95.5/23.5	96/24	96.5/24.5	97/25	95.5/25.5	96/26	96.5/26.5	97/27	
40	-2.19	-2.77	-2.19	-2.65	-1.33	-2.09	-1.51	-1.54	**2.03**
45	-2.86	-3.35	-2.73	-3.30	-2.18	-2.48	-1.97	-1.86	**2.59**
50	-3.20	-3.62	-2.98	-3.57	-2.63	-2.71	-2.10	-2.05	**2.86**
55	-3.40	-3.77	-3.04	-3.60	-3.00	-2.72	-2.26	-2.17	**2.99**
60	-3.29	-3.83	-2.96	-3.44	-3.12	-2.63	-2.30	-2.13	**2.96**
65	-3.18	-3.77	-2.86	-3.34	-3.25	-2.45	-2.30	-2.00	**2.89**
70	-2.96	-3.68	-2.67	-3.14	-3.38	-2.36	-2.35	-1.92	**2.81**
75	-2.81	-3.45	-2.40	-2.76	-3.26	-2.14	-2.16	-1.72	**2.59**

Supplementary Figure 5: Pseudo thermal anomalies converted from Vs anomalies using a conversion factor of -0.375 m/s^{o}C at 75-km **(a)** and 150-km **(b)** depths. The thermal anomaly is significantly high at shallower depth suggesting a deep thermal source unlikely.

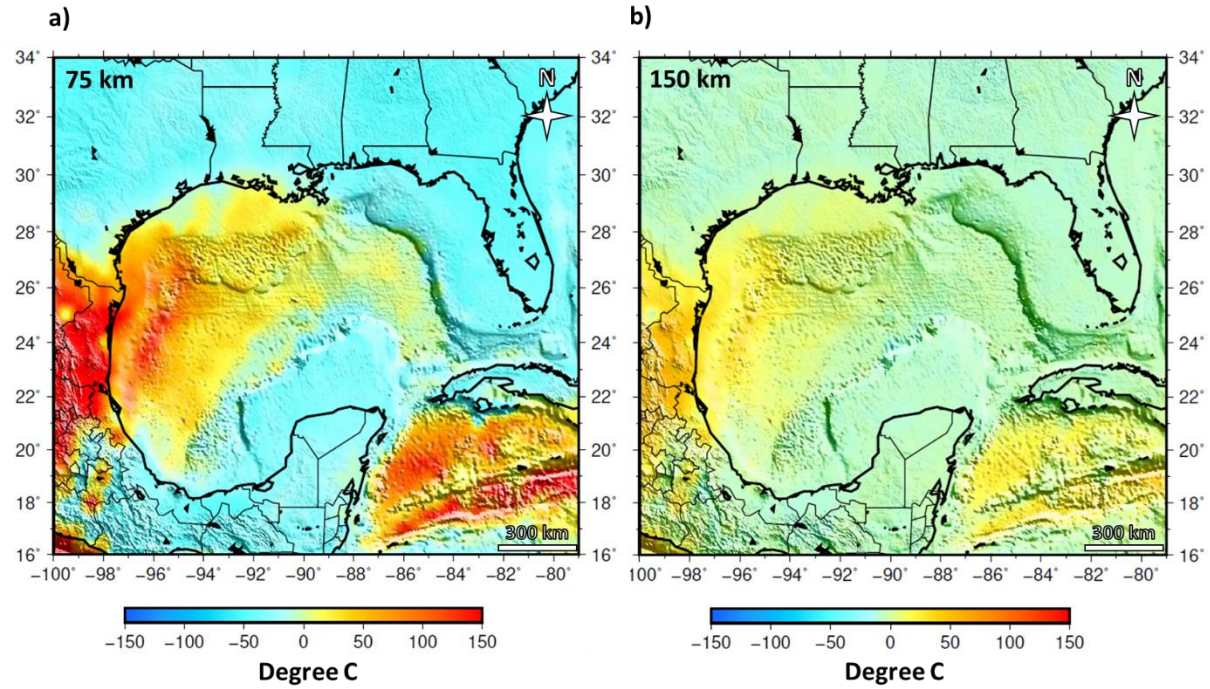

Supplementary Figure 6: Spatial correlation between variation in Moho depth and mantle boudinage. White arrows mark locations where the Moho exhibits a seaward dip. This is consistent with oblique shear-zones (black dashed lines) extending upward from the boudin necks and offset the base of the crust.

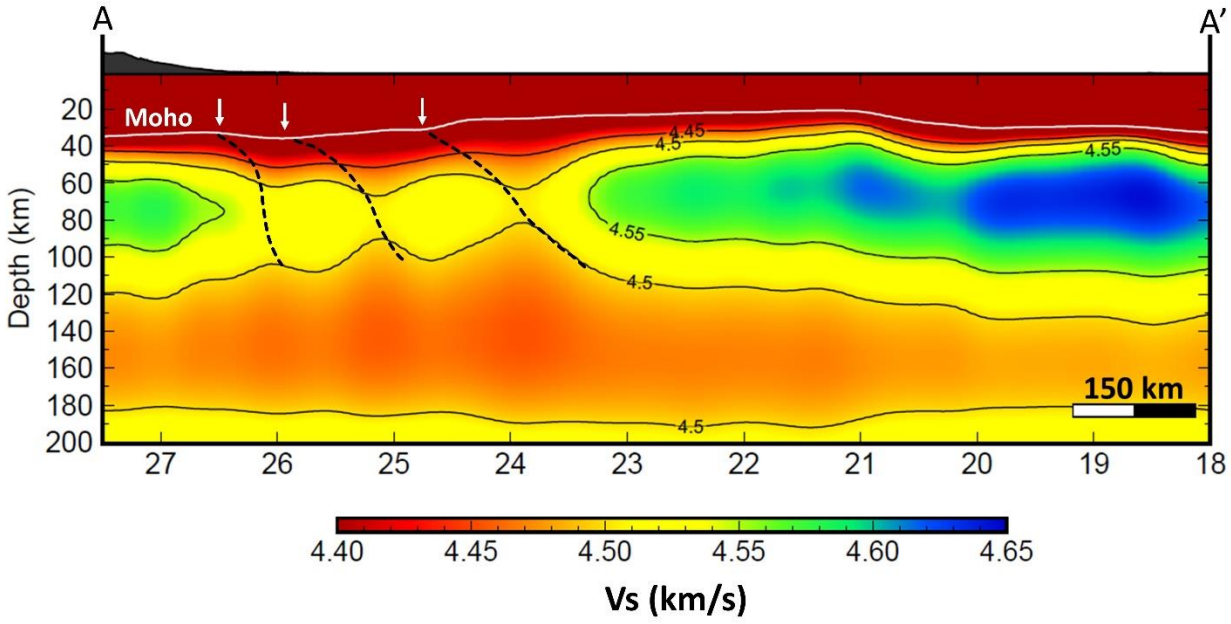

Supplementary Figure 7: Stretching beta factor of the crystalline crust calculated assuming an original thickness of 40 km. The white dashed outline is the 10-km thickness contour of crystalline crust. Grey arrows approximate width of the extended regions between the Ouachita fold belt (beta = 1) and the thickness contour. The arrows' lengths increase from west to east indicating a more widely distributed rift zone in this direction. Note that the extended terrain with beta factor >2 in the Yucatan margin is significantly narrower than that over the Gulf Coast margin displaying asymmetric rifting between these two conjugate margins.

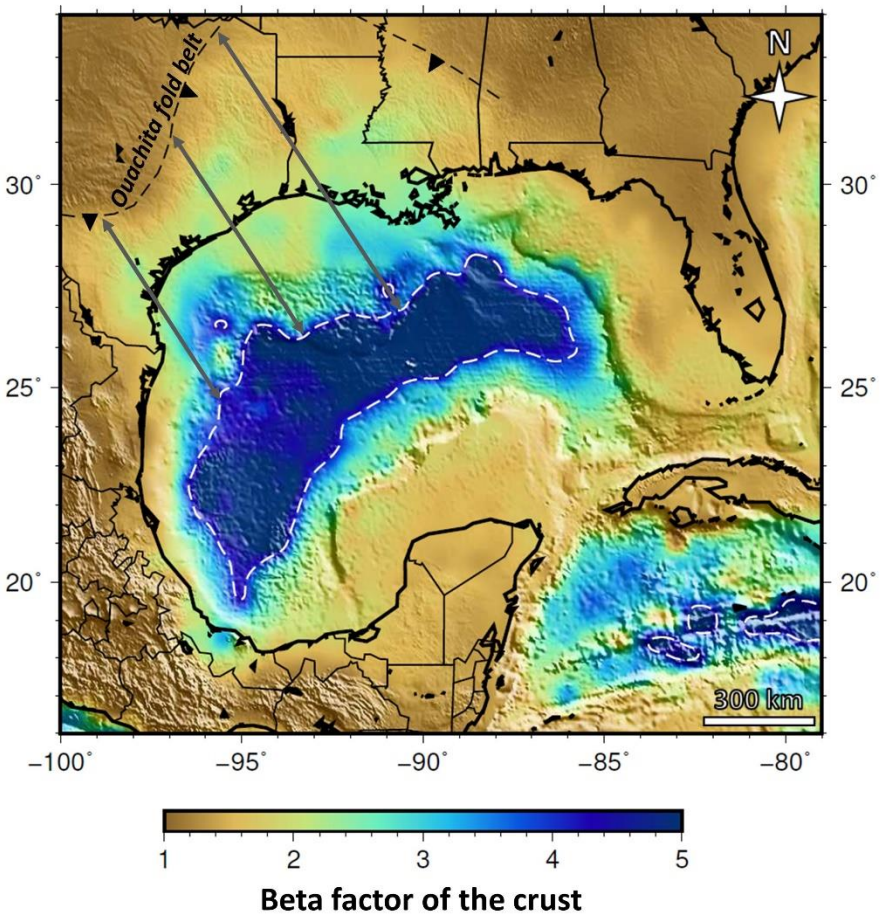

REFERENCES

Albuquerque Seismological Laboratory (ASL)/USGS. (2013). Central and Eastern US Network [Data set]. International Federation of Digital Seismograph Networks. https://doi.org/10.7914/SN/N4

Albuquerque Seismological Laboratory (ASL)/USGS. (2006). Caribbean USGS Network [Data set]. International Federation of Digital Seismograph Networks. https://doi.org/10.7914/SN/CU

Albuquerque Seismological Laboratory (ASL)/USGS. (1990). United States National Seismic Network [Data set]. International Federation of Digital Seismograph Networks. https://doi.org/10.7914/SN/US

Albuquerque Seismological Laboratory (ASL)/USGS. (1988). Global Seismograph Network - IRIS/USGS [Data set]. International Federation of Digital Seismograph Networks. https://doi.org/10.7914/SN/IU

Van Avendonk, H.J.A., Christeson, G.L., Norton, I.O., and Eddy, D.R., 2015, Continental rifting and sediment infill in the northwestern Gulf of Mexico: Geology, v. 43, p. 631–634, doi:10.1130/G36798.1.

Bureau of Economic Geology, The University of Texas at Austin. (2016). Texas Seismological Network [Data set]. International Federation of Digital Seismograph Networks. https://doi.org/10.7914/SN/TX

Casagli, A., Frezzotti, M.L., Peccerillo, A., Tiepolo, M., and De Astis, G., 2017, (Garnet)-spinel peridotite xenoliths from Mega (Ethiopia): Evidence for rejuvenation and dynamic thinning of the lithosphere beneath the southern Main Ethiopian Rift: Chemical Geology, v. 455, p. 231–248, doi:10.1016/j.chemgeo.2016.11.001.

Christeson, G.L., Avendonk, H.J.A. Van, Norton, I.O., Snedden, J.W., Eddy, D.R., Karner, G.D., and Johnson, C.A., 2014, Deep crustal structure in the eastern Gulf of Mexico: Journal of Geophysical Research, Solid Earth, v. 119, p. 6782–6801, doi:doi:10.1002/ 2014JB011045.

Eddy, D.R., Van Avendonk, H.J.A., Christeson, G.L., and Norton, I.O., 2018, Structure and origin of the rifted margin of the northern Gulf of Mexico: Geosphere, v. 14, p. 1804–1817, doi:10.1130/GES01662.1.

Eddy, D.R., Avendonk, H.J.A. Van, Christeson, G.L., Norton, I.O., Karner, G.D., Johnson, C., and Snedden, J.W., 2014, Deep crustal structure of the northeastern Gulf of Mexico: Implications for rift evolution and seafloor spreading: Journal of Geophysical Research: Solid Earth, v. 119, p. 6802–6822, doi:10.1002/2014JB011311.

Faul, U.G., and Jackson, I., 2005, The seismological signature of temperature and grain size variations in the upper mantle: Earth and Planetary Science Letters, v. 234, p.

Fletcher, R.C., and Hallet, B., 1983, Unstable extension of the lithosphere: a mechanical model for Basin-and- Range structure.: Journal of Geophysical Research, v. 88, p. 7457–7466, doi:10.1029/JB088iB09p07457.

Froidevaux, C., 1986, Basin and Range large-scale tectonics: constraints from gravity and reflection seismology: Journal of Geophysical Research, v. 91, p. 3625–3632.

Gerya, T. V., Bercovici, D., and Becker, T.W., 2021, Dynamic slab segmentation due to brittle-ductile damage interactions in the outer rise: Nature, v. 599, p. 2445–250.

Griffin, W.L., O'Reilly, S.Y., Afonso, J.C., and Begg, G.C., 2009, The composition and evolution of lithospheric mantle: A re-evaluation and its tectonic implications: Journal of Petrology, v. 50, p. 1185–1204, doi:10.1093/petrology/egn033.

Gueguen, E., Doglioni, C., and Fernandez, M., 1997, Lithospheric boudinage in the western Mediterranean back-arc basin: Terra Nova, v. 9, p. 184–187, doi:10.1046/j.1365-3121.1997.d01-28.x.

Hopper, J.R., and Buck, W.R., 1993, The initiation of rifting at constant tectonic force: role of diffusion creep: Journal of Geophysical Research, v. 98, p. 213–22

IRIS Transportable Array. (2003). USArray Transportable Array. International Federation of Digital Seismograph Networks. https://doi.org/10.7914/SN/TA1.

Jackson, I., Fitz Gerald, J.D., Faul, U.H., and Tan, B.H., 2002, Grain-size-sensitive seismic wave attenuation in polycrystalline olivine: Journal of Geophysical Research: Solid Earth, v. 107, p. ECV 5-1-ECV 5-16, doi:10.1029/2001jb001225.

Karato, S.I., and Wu, P., 1993, Rheology of the upper mantle: A synthesis: Science, v. 260, p. 771–778, doi:10.1126/science.260.5109.771.

Karen M. Fischer, Robert B. Hawman, & Lara S. Wagner. (2010). Southeastern Suture of the Appalachian Margin Experiment [Data set]. International Federation of Digital Seismograph Networks. https://doi.org/10.7914/SN/Z9_2010

Krauss, Z., and Menke, W., 2020, The Northern Gulf Anomaly: P- and S-wave travel time delays illuminate a strong thermal feature beneath the Northern Gulf of Mexico: Earth and Planetary Science Letters, v. 534, p. 116102, doi:10.1016/j.epsl.2020.116102.

Liu, W., Kung, J., and Li, B., 2005, Elasticity of San Carlos olivine to 8 GPa and 1073 K: Geophysical Research Letters, v. 32, p. 1–4.

MASE (2007): Meso America Subduction Experiment. Caltech. Dataset. doi:10.7909/C3RN35SP

Müntener, O., Manatschal, G., Desmurs, L., and Pettke, T., 2009, Plagioclase peridotites in ocean-continent transitions: Refertilized mantle domains generated by melt stagnation in the shallow mantle lithosphere: Journal of Petrology, v. 51, p. 255–294, doi:10.1093/petrology/egp087.

National Centre for Seismological Research (CENAIS Cuba). (1998). Servicio Sismologico Nacional de Cuba [Data set]. International Federation of Digital Seismograph Networks. https://doi.org/10.7914/SN/CW

O'Reilly, S.Y., and Griffin, W.L., 2013, Mantle metasomatism, *in* Harlov, D.E. and Austrheim, H. eds., Metasomatism and the Chemical Transformation of Rock-The Role of Fluids in Terrestrial and Extraterrestrial Processes, Springer-Verlag, p. 471–533.

Pérez-Gussinyé, M., Morgan, J.P., Reston, T.J., and Ranero, C.R., 2006, The rift to drift transition at non-volcanic margins: Insights from numerical modelling: Earth and Planetary Science Letters, v. 244, p. 458–473, doi:10.1016/j.epsl.2006.01.059.

Ranalli, G., Piccardo, G.B., and Corona-Chávez, P., 2007, Softening of the subcontinental lithospheric mantle by asthenosphere melts and the continental extension/oceanic spreading transition: Journal of Geodynamics, v. 43, p. 450–464, doi:10.1016/j.jog.2006.10.005.

Smith, R.B., 1977, Formation of folds, boudinage, and mullions in non-Newtonian materials: Bulletin of the Geological Society of America, v. 88, p. 312–320, doi:10.1130/0016-7606.

Stern, R.J., and Dickinson, W.R., 2010, The Gulf of Mexico is a Jurassic backarc basin: Geosphere, v. 6, p. 739–754, doi:10.1130/GES00585.1.

Stern, R.J., Anthony, E.Y., Ren, M., Lock, B.E., Norton, I., Kimura, J.I., Miyazaki, T., Hanyu, T., Chang, Q., and Hirahara, Y., 2011, Southern Louisiana salt dome xenoliths: First glimpse of Jurassic (ca. 160 Ma) Gulf of Mexico crust: Geology, v. 39, p. 315–318, doi:10.1130/G31635.1.

VEOX (2010): Veracruz-Oaxaca Subduction Experiment. Caltech. Dataset. doi:10.7909/C3MW2F2C

Wang, H., Hunen, J. van, and Pearson, D.G., 2015, The thinning of subcontinental lithosphere: The roles of plume impact and metasomatic weakening: Geochemistry Geophysics Geosystems, v. 16, p. 1156–1171.

Yamasaki, T., 2004, Localized rheological weakening by grain-size reduction during lithospheric extension: Tectonophysics, v. 386, p. 117–145, doi:10.1016/j.tecto.2004.05.006.

Yao, Y., and Li, A., 2016, Lithospheric velocity model of Texas and implications for the Ouachita orogeny and the opening of the Gulf of Mexico: Geophysical Research Letters, v. 43, p. 12,046-12,053, doi:10.1002/2016GL071167.

Zhu, H., Stern, R.J., and Yang, J., 2020, Seismic evidence for subduction-induced mantle flows underneath Middle America: Nature Communications, v. 11, doi:10.1038/s41467-020-15492-6.